Displacement-based seismic performance assessment of multi-span steel truss bridges

DISPLACEMENT-BASED SEISMIC PERFORMANCE ASSESSMENT OF MULTI-SPAN STEEL TRUSS BRIDGES

Andrea Nettis[1], Pietro Iacovazzo[1], Domenico Raffaele[1], Giuseppina Uva[1], Jose M. Adam[2]

1 Department of Civil, Environmental, Land, Building Engineering and Chemistry, Polytechnic University of Bari, Bari, Italy
2 ICITECH, Universitat Politècnica de València, Valencia, Spain

Correspondence to: Andrea Nettis (andrea.nettis@poliba.it)

Abstract. Simplified mechanics-based approaches for the seismic performance analysis are used for the risk assessment of large bridge portfolios. This study evaluates the applicability and effectiveness of displacement-based assessment (DBA) and nonlinear static procedures for multi-span railway steel truss bridges. Although built in the first part of the last century, these historical bridges are currently in service within the European railway networks, and their seismic performance is poorly investigated in the literature. Direct DBA algorithms and pushover-based procedures aimed at seismic performance assessment and fragility analysis of bridges are presented and tested within a set of case studies parametrically generated by using an archetype steel truss bridge. The first part of this study focuses on the seismic analysis of steel braced towers which, in many situations, compose the substructure of steel truss multi-span bridges. A simplified pseudo-pushover and an accurate equivalent viscous damping formulation are proposed to be used for the approximate performance displacement assessment of these structural components. The second part discusses the accuracy of the investigated approaches for multi-span steel truss bridges through comparisons with nonlinear time history analysis. The results of the parametric analysis are used to propose recommendations for an appropriate DBA or pushover-based strategy for the deterministic performance assessment and fragility analysis with reference to the damage state of the supporting towers or bridge serviceability in terms of superstructure transverse deformation.

Keywords. displacement-based seismic assessment, steel truss bridges, fragility analysis, pushover analysis, capacity spectrum method, nonlinear time history

1. Introduction

The research activity for the understanding and reduction of disaster risk for people and assets, including transport infrastructure systems, is strongly endorsed by the United Nations within the 2030 Agenda for Sustainable Development [1] and within the Sendai Framework for Disaster Risk Reduction 2015–2030 [2]. The serviceability of a transport infrastructure network can be severely affected by an inadequate structural response of existing bridges subjected to natural or man-made hazards, as proved by recent catastrophic events (e.g. I-35W bridge in Minnesota [3], the Kinzua Bridge in Pennsylvania [4]). In earthquake-prone countries, the seismic risk assessment of existing bridge portfolios is of increasing concern for transport authorities to address targeted retrofitting and increase the resilience of the transport networks. Most of these critical structures may exhibit an inadequate seismic performance subjected to earthquake-induced ground shaking since these were mostly designed in the past without anti-seismic requirements. Given the high number of existing bridges to be inspected and assessed, refined modelling and analysis methodologies, such as nonlinear time-history analysis (NLTHA), are not practical because of their large demand for computational effort [5]. Various research studies (e.g. [6–8]) focused on the development and testing of more efficient simplified seismic analysis approaches suitable for large bridge portfolio analysis. Nonlinear static procedures represent a simplified alternative displacement-based performance assessment approach with respect to NLTHA. These are based on pushover analysis of the structure under study and approximate methods for performance displacement prediction based on its equivalent SDoF response [6]. The applicability of nonlinear static approaches was widely investigated for reinforced concrete (RC) multi-span bridges [9–13], which are arguably the most frequent bridge typology in Europe. These studies concluded that conventional pushover analysis with an invariant first mode-based load pattern can be successfully applied to regular bridges. For irregular bridges, whose seismic response is typically affected by strong higher-mode contributions or by significant damage-induced variability of modal shapes, more complex algorithms for pushover analysis are proposed in the abovementioned studies (e.g. multi-modal or adaptive force- or displacement-based load patterns [14–16]). Based on early studies on direct displacement-based design and assessment by Priestley et al. [17], various research efforts focused on proposing direct displacement-based assessment (DBA) approaches for predicting the pier-specific displacement demand for RC bridges in a given damage state (DS) [6,8,18,19].

To the authors' knowledge, there are no studies in the literature that test these simplified methodologies for the commonly used European steel truss bridges. These are mainly historical bridges, built during the construction of the transport network between the second half of the 19th century and the first decades of the 20th [20]. A large number of these old bridges are still

in service and should be subjected to structural assessment with respect to the current code prescriptions (e.g. traffic actions and natural hazards) and, if necessary, retrofitted. Although these bridges are worthy of refined analysis, given their considerable historical value and structural complexity, testing the applicability of simplified methods on these bridges is important for addressing seismic risk-based prioritisation of bridge portfolios, modelling the vulnerability of transport networks for the time- or scenario-based loss calculation and resilience analysis of populated contexts.

According to the classification reported within the *Seismic Retrofitting Guidelines for Complex Steel Truss Highway Bridges* [21], this category includes bridges whose superstructure components are structural truss systems composed of axially loaded straight steel members connected in triangular patterns. The superstructure is commonly composed of two truss girders consisting of two longitudinal (upper and lower) chords connected by diagonal and vertical frames. The two truss beams are connected by secondary bracing systems, aimed at resisting seismic and wind loads, and floor beams supporting stringers and the railway plane. The superstructure of multi-span truss bridges consists of simply supported adjacent trusses (i.e. isostatic superstructure) or a continuous (i.e. hyperstatic superstructure) truss superstructure. The substructure is generally composed of steel braced towers or unreinforced masonry/RC walls. According to Ref. [21], the transverse stiffness of the truss superstructure is lower than the stiffness of steel braced towers or massive wall piers. This feature limits the capacity of the superstructure to transfer seismic inertia forces between the substructure components and leads to significant higher-mode contributions in the seismic response. Studies on this bridge typology are few and mainly deal with the fatigue response of truss spans characterised by riveted connections. Several studies [22–25] described experimental campaigns on dismantled steel truss spans to analyse the fatigue response of the superstructure components and particularly of the riveted connections under cyclic loading. To the authors' knowledge, the study by Yilmaz & Çalayan [26] is the only recent work on the seismic fragility of a multi-span steel truss railway bridge. It included the fragility analysis of a case-study bridge in Turkey, discussing the efficiency of different intensity measures.

This paper deals with the applicability and effectiveness of DBA and nonlinear static procedures for the seismic assessment of multi-span steel truss bridges with steel braced towers. Section 2 presents the simplified analysis methodologies, including novel and state-of-the-art DBA algorithms aimed at the direct seismic performance assessment under a given seismic action, pushover analyses coupled with capacity spectrum method (CSM) [27] and extensions to perform a probabilistic seismic assessment considering the record-to-record variability. The analysed direct DBA algorithms allow for considering higher-

mode contributions. An existing historical European steel truss railway bridge is identified as an archetype structure (Section 3). The discussion of the results is organised into two parts. The first (Section 4) addresses some applicability issues of DBA or nonlinear static procedures concerning steel truss bridges, as opposed to RC bridges thoroughly analysed in the literature. These issues refer to the seismic assessment of steel towers considering the simplified calculation of force-displacement relationships, the definition of displacement-based damage states and equivalent viscous damping formulations to be used to approximate the hysteretic dissipation. The second discussion (Section 5) is focused on the effectiveness of the investigated approaches for the seismic performance assessment and fragility analysis on six parametric continuous-superstructure steel truss bridges, considering the ultimate damage state of the supporting towers or the bridge serviceability measured by the transverse deformations of the superstructure. The differences in seismic behaviour of steel truss bridges with respect to ordinary RC bridges are highlighted, motivating the need for specific investigations focused on this bridge typology. Specific recommendations to appropriately apply DBA and nonlinear static procedures for multi-span steel truss bridges are proposed.

2. Description of DBA and nonlinear static procedures and extension for fragility analysis

In this section, the DBA and nonlinear static procedures adopted for the seismic performance assessment (i.e. calculation of displacement demand under a given seismic action) of steel truss bridges are described. First, a state-of-the-art on DBA algorithms for bridges and a description of the adopted DBA algorithms, which are adapted for performing a direct performance displacement calculation, is illustrated. The investigated nonlinear static procedures, based on pushover analysis and CSM, are also presented. Finally, an extension of the adopted simplified analysis methodologies for fragility analysis is described.

2.1. Direct DBA approaches

Sadan et al. [8] proposed the first version of DBA for continuous-deck RC multi-span bridges based on an iterative eigenvalue analysis. This methodology was slightly modified by Gentile et al. [19], who proposed an alternative DBA approach based on simple iterative equivalent static analysis. Both approaches suit the seismic analysis in the transverse direction, where two load paths combine (i.e. the seismic action is absorbed by the deck-abutment systems and by the piers). To emphasize the simplicity of the algorithm, a simplified modelling approach can be used: the bridge is modelled by an equivalent elastic beam based on inelastic supports representing the piers and abutments [8,13,19]. According to recent studies [18,19], the DBA can also be straightforwardly applied for analysing the longitudinal response of straight multi-span bridges. Since the superstructure can

be assumed axially rigid in the longitudinal direction, the seismic response of the bridge can be represented by the response of the resisting substructure members (where a fixed connection to the superstructure is placed) working in parallel. In this case, the process is simpler than for the transverse direction since no iterations are required. Additionally, past studies [6,18,28] guided the application of DBA algorithms for simply-supported (isostatic) multi-span bridges. In these cases, each substructure member can be isolated and analysed separately.

These DBA algorithms allow the analyst to calculate the limit state displacement profile of the investigated bridge given the damage state displacement of a critical substructure member. A final pass/fail assessment is performed via capacity-demand ratios calculated by comparing the elastic displacement capacity of the equivalent SDoF system of the bridge in limit state condition and the elastic demand (represented by 5%-damped response spectra). Unlike the abovementioned versions, the DBA algorithm adopted in this study allows for the direct displacement demand calculation on the bridge components under a given seismic action. It is based on the approach by Gentile et al. [19] that proposed a displacement-based pseudo pushover subjected to the CSM to enable the seismic demand computation. The presented DBA methodology, illustrated in **Errore. L'origine riferimento non è stata trovata.**, is an evolved solution with respect to the DBA proposed in Ref. [19] since it synthesises the combination of displacement-based pseudo-pushover and CSM in a single efficient iterative algorithm. This modification enables also the use of different procedures to combine higher-mode contributions as explained below.

Figure 1 presents the workflow. The first step requires the definition of the input response spectrum in pseudo-spectral acceleration-displacement format and the characterisation of the abovementioned simplified beam model. The force-displacement relationships of the substructure members should be calculated and assigned to the inelastic supports. An initial modal analysis is performed by assuming a tentative value of the secant-to-target-displacement stiffness k_i for each *i-th* substructure member. The adoption of the secant-to-yielding stiffness is recommended as an initial assumption. The modal shapes which are deemed to significantly contribute to the performance displacement profile should be selected. It is recommended to select all the modes having more than 5% of participating mass. However, according to Sadan et al. [8], only the first mode can be selected if the corresponding participating mass is higher than 70%. Subsequently, a first tentative performance displacement profile (Δ_i for each node) should be calculated. For this aim, the modal displacement profiles composed of Δ_{ij} for each mode j are calculated via Equation (1), where $S_a(T_j)$ is the elastic spectral demand displacement

for the period T_j, Γ_j is the modal participation factor and ϕ_{ij} is the modal component. A modal superposition is performed by using the complete quadratic combination (CQC) to calculate Δ_i.

$$\Delta_{ij} = \Gamma_j S_d(T_j)\phi_{ij} \quad (1)$$

Iterations are carried out to update Δ_i accounting for the reduction in the spectral demand due to the hysteretic dissipation of the structural members (step 5 in Figure 1). Two alternative approaches are adopted in this study for this scope.

The first approach is based on the use of the Effective Mode Shape according to Kowalsky [29]. This approach is applied as follows and identified hereafter as iterative effective mode shape (IEMS).

1. Calculation of the equivalent SDoF system corresponding to the bridge in performance displacement condition in terms of effective displacement Δ_{eff} (Equation (2)), total base shear ($V_b = \sum V_i$), effective mass m_{eff}, effective period T_{eff} (Equation (3)), and equivalent viscous damping ξ_{eff} (Equation (4), ξ_{sup} is the elastic damping associated to the superstructure). For this latter, an appropriate value of equivalent viscous damping (ξ_i) to approximate the dissipation associated with the hysteretic response of the single substructure member should be adopted [17].
2. The equivalent SDoF displacement demand at the effective period $S_d^{\xi}(T_{eff})$ considering the equivalent viscous damping is calculated by multiplying the elastic spectral demand displacement $S_d(T_{eff})$ for the corresponding spectral reduction factor, η_{eff} (Equation (5)).
3. The initial Δ_{eff} is compared to $S_d^{\xi}(T_{eff})$ for the compatibility check with respect to the initial assumption. If the convergence is not satisfied, another iteration is performed. A new performance displacement profile Δ_i^{ξ} is calculated via Equation (6) where the normalised displacement profile ϕ_i and the corresponding modal participation factor Γ_{eff} are used. Δ_i^{ξ} is adopted for the new iteration repeating steps 1 to 3. A displacement tolerance of 1 mm is adopted in this study.

$$\Delta_{eff} = \sum_{i=1}^{N} \frac{m_i \Delta_i^2}{m_i \Delta_i} \quad (2)$$

$$T_{eff} = 2\pi \sqrt{\frac{m_{eff}}{k_{eff}}} \quad where \quad k_{eff} = \frac{V_b}{\Delta_{eff}}, m_{eff} = \frac{\sum_{i=1}^{N} m_i \Delta_i}{\Delta_{eff}} \quad (3)$$

$$\xi_{eff} = \frac{\xi_{sup}\,\Delta_{eff}(V_1 + V_N) + \sum_{i=1}^{N} \xi_i \Delta_i V_i}{\Delta_{eff}(V_1 + V_N) + \sum_{i=1}^{N} \Delta_i V_i} \tag{4}$$

$$\eta_{eff} = \sqrt{0.07/\left(0.02 + \xi_{eff}\right)} \tag{5}$$

$$\Delta_i^{\xi} = \Gamma_{eff} S_d^{\xi}\left(T_{eff}\right)\phi_i \tag{6}$$

The second approach is more refined than the first. While the IEMS considers the damping associated with the global displacement profile, this second approach accounts for the equivalent viscous damping associated with each of the displacement profiles associated with each mode. It is based on well-known response spectrum analysis and the study by Perdomo & Monteiro [13]. It is identified as iterative response spectrum analysis (ITERSA) and is applied as follows.

1. The equivalent SDoF system related to each mode j is calculated in terms of effective displacement $\Delta_{eff,j}$ via Equation (2) using Δ_{ij}. The total base shear $V_{b,j}$, effective mass $m_{eff,j}$, effective period $T_{eff,j}$ and equivalent viscous damping $\xi_{eff,j}$ are calculated (by applying Equation (3) and (4) for each *j-th* mode).
2. The equivalent SDoF displacement demand related to each mode $S_d^{\xi}(T_j)$ is calculated by multiplying the elastic spectral demand displacement $S_d(T_j)$ for the corresponding specific-mode spectral reduction factor η_j (Equation (5)). This allows for a recalculation of the performance displacement profiles Δ_{ij}^{ξ} to be associated with each mode accounting for specific-mode damping by applying Equation (1) using $S_d^{\xi}(T_j)$ instead of $S_d(T_j)$.
3. A new global performance displacement profile Δ_i^{ξ} is also obtained by combining Δ_{ij}^{ξ} via the CQC combination. This is compared to the first tentative Δ_i, checking the convergence according to a pre-determined value of tolerance. If the convergence is satisfied, the process is completed; if not, other iterations should be performed by using Δ_{ij}^{ξ} as a tentative estimate of specific-mode displacement profile.

It is worth noting that the stabilised performance displacement profile obtained by this iterative approach reflects the "elastic" modal shapes obtained by the first modal analysis which is performed by using secant-to-yielding stiffness. To consider the modifications of the modal shapes which occur according to the increasing inelastic demand on the resisting structural members, another iterative process is performed to conclude the DBA whether IEMS and ITERSA are performed. According to the flowchart in Figure 1 (step 6), the shear demand V_i^{ξ} is interpolated by using the force-displacement relationships

associated with each member, the corresponding k_i^{ξ} is calculated and compared to the initial stiffness assumption. The convergence is checked by adopting a pre-determined tolerance value. If the convergence is not reached the process is repeated from step 3 of Figure 1 until convergence on secant-to-target-displacement stiffness is reached.

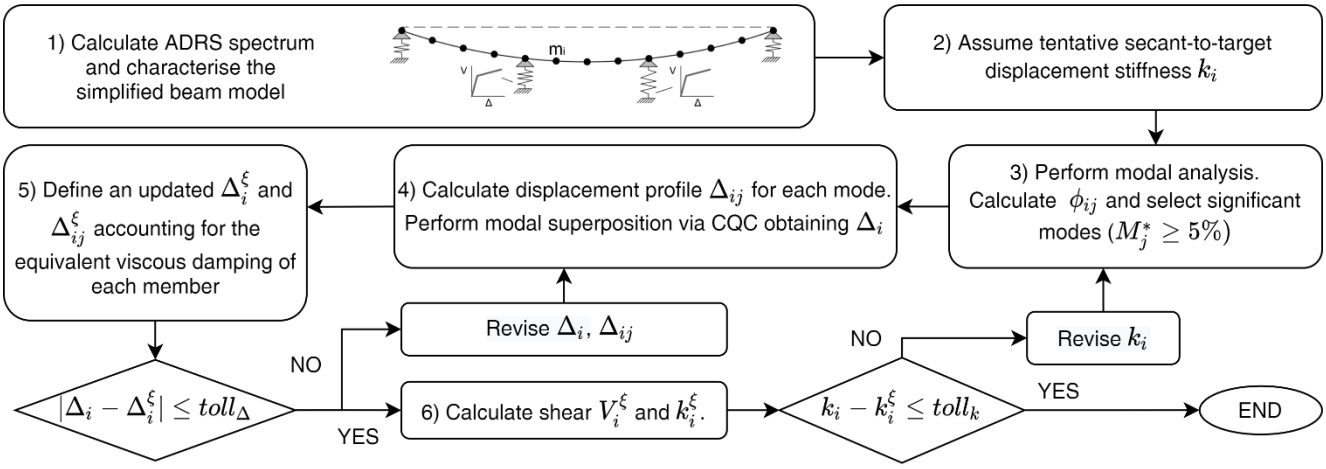

Figure 1. Flowchart of the direct DBA approach for calculating the displacement demand under a given seismic action.

The presented direct DBA is a multi-modal approach, accounting for the contribution of higher modes. It is demonstrated in the following sections (see Section 5.2) that this feature is essential for analysing the seismic response of steel truss bridges which exhibit an "irregular" response. Moreover, the algorithm is "adaptive", considering the updating of the modal shapes for increasing inelastic demand on the substructure members.

Finally, a simpler DBA algorithm is introduced and identified as simplified iterative response spectrum analysis (S-IRSA). This last approach coincides with the DBA with ITERSA but excludes the last iterative process for updating the modal shapes (i.e. it is not adaptive) and performs the performance displacement assessment by using the elastic modal shapes. It is simply performed by applying steps 1 to 5 of Figure 1. Only a first eigenvalue analysis, assuming the secant-to-yielding stiffness (step 2 of Figure 1) is performed and the elastic modal shapes are combined to introduce the iterative process for calculating the stabilised damped displacement demand on the bridge components. The S-IRSA is used to investigate if it is worth accounting for the modifications of modal shapes for increasing inelastic demand within the analysis of steel truss multi-span bridges.

While, as mentioned above, the application of DBA algorithms is widely addressed for RC bridges, some hindrances arise within the application on steel truss bridges. These are related to: 1) the absence of simplified procedures to compute force-displacement relationships for steel braced towers; 2) the lack of reliable equivalent viscous damping formulations to

approximate the hysteretic dissipation of steel braced towers subjected to cyclic loads. The study reported in the following Section 4 is aimed to address these issues.

2.2. Nonlinear static procedures

The effectiveness of the proposed direct DBA for steel truss bridges is discussed with reference to conventional nonlinear static procedures for displacement-based seismic performance assessment. These are based on the pushover analysis of the investigated structure and approximate methods for performance displacement prediction based on the inelastic equivalent SDoF response of the structure [6]. Several approximate methods for inelastic performance displacement prediction exist [30] such as the N2 method [31,32] and the capacity spectrum method (CSM) [33]. The CSM, implemented in different guidelines (e.g., ATC-40 [34] and FEMA-440 [35]), calculates the target displacement of inelastic systems as the displacement of equivalent elastic SDoF systems having secant-to-target-displacement stiffness and higher viscous damping. Similarly to the abovementioned DBA, the CSM approximates the hysteretic dissipation of inelastic systems by using the equivalent viscous damping. Therefore, as for the DBA, the application of CSM for steel truss bridges requires the identification of appropriate equivalent viscous damping formulations.

The nonlinear static approaches adopted in this study consist of pushover analyses carried out by using a first-mode-proportional and a uniform invariant load pattern. These methodologies are hereafter defined as PUSHm and PUSHu, respectively. The pushover curves are converted in capacity spectra related to an equivalent SDoF system and are subjected to the CSM algorithm adopting consistent formulations for equivalent viscous damping with respect to the DBA. Particularly, the modified CSM algorithm proposed by Nettis et al. [36], which can be used for both code-based and real response spectra, is applied.

2.3. Extension for fragility analysis

Fragility functions represent the probability to reach or exceed a given DS for a given earthquake-induced ground shaking intensity and are commonly expressed by lognormal cumulative distribution functions (e.g. [37,38]). The studies [6,18] provided simplified procedures for fragility analysis based on DBA and nonlinear static procedures where the central value is calculated estimating the seismic intensity measure (IM) corresponding to the equivalent elastic DS capacity. In these studies,

since smooth code-based response spectra (which do not allow for the explicit consideration of record-to-record variability) are used, conventional literature values of variance should be introduced in the fragility functions.

Conversely, the procedure applied in the present study for fragility analysis allows the user for the direct consideration of the record-to-record variability. A suite of ground-motion records is preliminary selected, the corresponding response spectra are computed and the IM of interest is extracted for each record. The abovementioned DBA algorithms are adopted to calculate appropriate engineering demand parameters (EDP), which represent the performance of the bridge under the selected ground-motion suite represented by real (as-recorded) response spectra. A dataset of edp_{gm}- im_{gm} pairs computed for each ground motion gm is obtained. To determine the probabilistic seismic demand model, a power-law model ($EDP = aIM^b$), representing the continuous relationship between EDP and IM is computed [38]. The fragility function, $P(EDP \geq edp_{DS}|IM)$, is expressed by the normal cumulative distribution function $\phi(\cdot)$ in Equation (7) where edp_{DS} is the EDP corresponding to a given DS. The parameters a and b are calculated by fitting a linear model on the edp_{gm}- im_{gm} pairs transformed in the $\log EDP - \log IM$ plane [39] through regression analysis resorting to the least square method. The dispersion σ is also calculated through Equation (7). The same strategy can be adopted by using the EDPs calculated by means of the nonlinear static procedures described in subsection 2.2. According to Bakalis and Vamvatsikos [37], this approach suits for cloud analysis [36,39] (in which the input record suite is composed by a given number of un-scaled ground motions) and few-stripe analysis [40] (which adopts a low number of "stripes" of records having the same IM).

$$P(EDP \geq edp_{DS}|IM) = 1 - \phi\left(\frac{\ln edp_{DS} - \ln a\ im^b}{\sigma}\right); \sigma = \sqrt{\frac{\sum_{gm=1}^{N}\left(\ln edp_{gm} - \ln a\ im_{gm}^b\right)^2}{N-2}} \quad (7)$$

3. Case-study bridges, modelling assumptions and seismic action

3.1. Description of the archetype bridge

An archetype steel truss bridge is selected to introduce a parametric analysis. This is a multi-span truss bridge built between 1913 and 1915 and still in service within the Spanish railway network. The superstructure is a continuous truss having 42m-long spans and consisting of two lateral Pratt-type truss beams. These are composed of built-up members, measuring a height equal to 4 m from the top of the bearings to the top of the upper chords. The upper and lower chords exhibit a T-shaped cross-section as shown in Figure 2. Two steel braced towers constitute the substructure system. The first is 18.60 m-high and the X-

bracing system is arranged in five panels, while the second exhibits a height equal to 11.88 m and three braced panels (Figure 2). The diagonals exhibit a T-shaped cross-section composed of coupled angles, while the horizontal braces are battened members composed of two pairs of coupled angles with steel plates as battens. At the top of the towers, 0.75 m-high beams are placed to support the bearing devices.

The legs are battened members: two built-up C-shaped parallel chords are connected by steel plates, one per 0.85 m, creating an open-box cross-section. Rivets are used to connect the different steel elements in each built-up member and for the connections between the members (e.g. the bracing systems to the gusset plates and legs). At the bottom of the steel towers, steel anchor bolts attach the legs to the masonry foundations. The bearing devices, recently replaced during a recent retrofit intervention, are confined elastomeric bearings preventing relative displacements between the superstructure and the substructure members in the transverse direction. Shock transmitters are also present to ensure the transmission of seismic forces from the superstructure to the towers. Further information about the analysed case study is reported in previous studies [25,41].

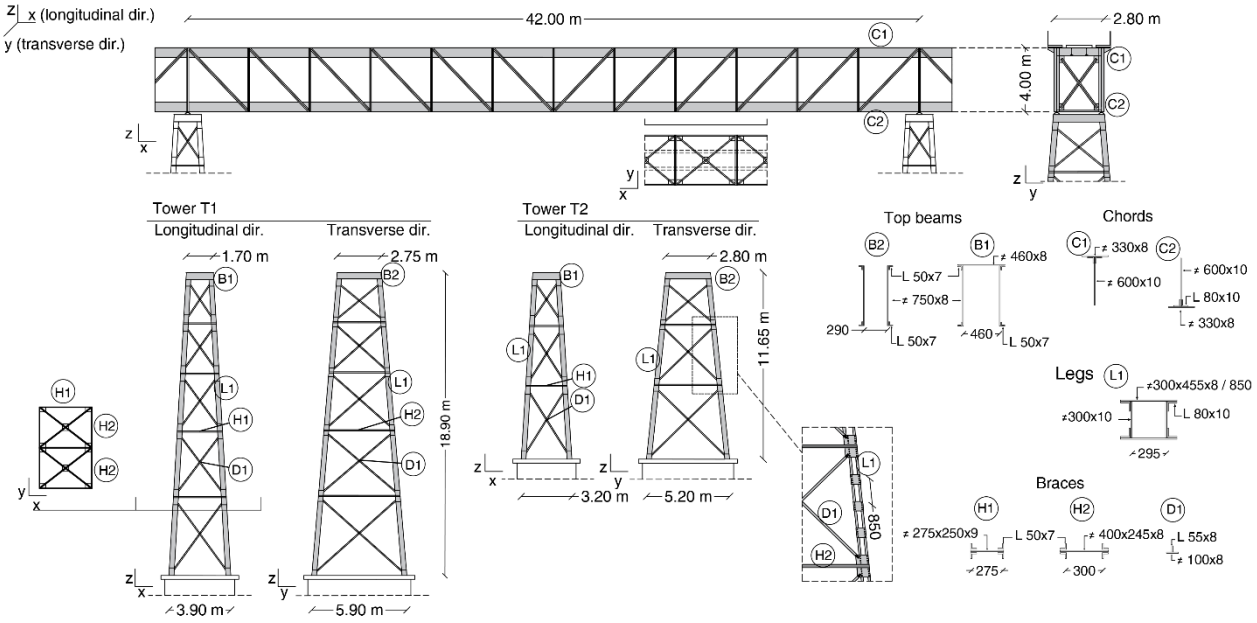

Figure 2. Geometric and constructive features of the archetype bridge.

3.2. Modelling strategy

Numerical models are created using the SAP2000 software package [42] and subjected to pushover analyses and NLTHA. The modelling strategy is graphically shown in Figure 3. The truss superstructure is modelled as a spine model by using an elastic frame whose flexural inertial characteristics are calculated considering a cross-section composed of the upper and lower chords of the truss beams (the contribution of the bracing members of the superstructure is neglected). Preliminary comparisons are performed to validate this simplified spine-modelling approach with respect to a refined tri-dimensional model of the truss superstructure. Modal analyses show that the simplified spine-model appropriately reflects the modal properties obtained by using the refined modelling approach provided that an appropriate mass discretisation of the superstructure is adopted. Therefore, each single-span superstructure frame is discretised in seven segments (i.e. 1 node/6 meters). The mass is calculated as the gravity loads plus the 20% of the traffic railway loads (calculated according to [43]).

The steel braced towers are modelled as follows: the legs and the top beams are represented by linear frame elements, while the diagonal and horizontal braces are modelled via nonlinear *two-nodes-link* elements. Fixed restraints are placed at the base of the legs (neglecting the soil-foundations interaction). Plastic hinges equipped with axial load-flexure interaction domains are used for modelling the nonlinear response of the legs, while simple flexural plastic hinges are assigned to the top beams. Shear hinges are also placed at the mid-length of the legs. Considering the recommendations by Eurocode 3 (EC3)-part 1 [44] and by the guidelines in [21] and the width-to-thickness ratios of the different plates and angles, the cross-sections of the built-up members can be classified as "compact" (Class 1 of the EC3) and local buckling phenomena are excluded.

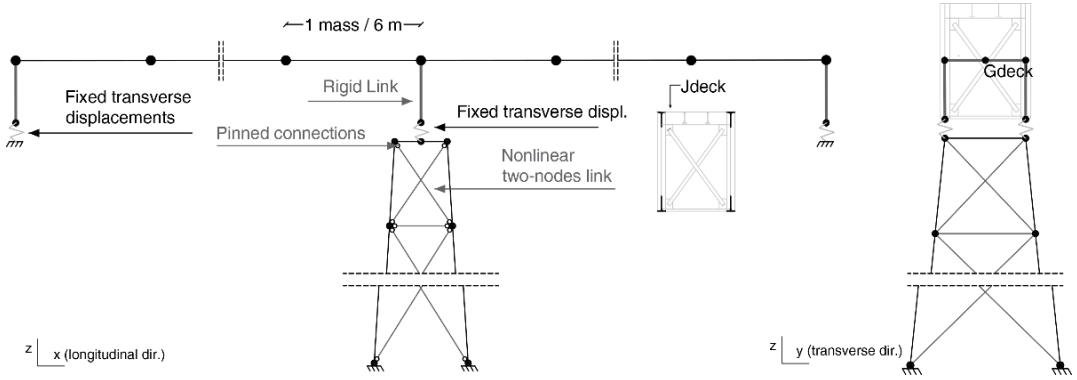

Figure 3. Modelling strategy for steel truss bridge case studies.

A simplified approach is used for calculating the axial load-flexure interaction domains for battened members accounting for lateral buckling. The compression strength N_c of the battened members is calculated considering the global buckling and the local buckling of the portion of longitudinal C-shaped profiles between the battens. For the former, a value of effective

slenderness accounting for the shear-induced flexibility is used. The tensile strength N_t is calculated using the net section area (i.e. the gross cross-section area excluding the rivet holes) of the longitudinal profiles only. The axial-load domain is discretised in several intervals $[N_i; N_{i+1}]$ between the maximum N_t and minimum N_c strength capacity. Varying N_i, the corresponding flexural strength is calculated according to the recommendations in Ref. [45]. For each compressive N_i, the minimum between the moment causing buckling of the single longitudinal C-shaped profile and the plastic moment of the cross-section is used as ultimate strength. This calculation is performed in both the flexure directions. The guidelines in Ref. [21] suggest adopting appropriate limitations for the ultimate ductility capacity of built-up steel members if no experimental tests or refined plastic analysis are performed. In this study, a maximum rotational ductility equal to 2 is used, corresponding to a severe damage condition (see subsection 4.2). This value is linearly reduced from 2 to 0, for compressive axial-load ratio included in $[0.5A_s\, f_y, A_s\, f_y]$ where A_s is the gross area of the cross-section, f_y is the steel yielding strength [46,47]. Shear hinges are also modelled considering the minimum between the ultimate plastic shear strength of the whole member and the shear force inducing axial buckling or yielding of the battens. Preliminary analyses according to Ref. [44] show that for both the battens and longitudinal profiles, shear buckling failures are excluded. A pinned connection between the legs and the bracing members is considered in the numerical model and, therefore, an axial-load-induced nonlinear response is associated with the diagonal and horizontal bracing members. The compression strength is calculated as the critical buckling load, which is largely lower than the plastic compressive stress, given the high slenderness ratio of the members, whereas the tensile strength is calculated considering the net section. The cyclic response of the bracing members is modelled according to Ref. [48]: the *pivot* hysteresis rule ($\alpha_1 = 100,\ \alpha_2 = 0.1,\ \beta_1 = 0.02,\ \beta_2 = 0.4,\ \eta = 0$) is selected for the *two-nodes-link* modelling the braces.

It is worth mentioning that a strength-based verification of the critical components, such as the riveted connections between the members or the anchorage devices connecting the legs to the foundation, should be performed to prove the validity of the adopted modelling strategy. This can be carried out following the recommendations in Ref. [21] by post-processing the seismic analysis results, but it is not significant with respect to the scope of this study. However, according to the experimental tests by Bertolesi et al. [41], the failure of the rivets is reasonably neglected for these case studies.

As anticipated in Section 2, the DBA procedures use a simplified modelling strategy where the truss superstructure is modelled by an equivalent beam model (Figure 1, step 1) and the steel braced towers are represented by inelastic supports. The mechanical features and mass discretisation of the simplified beam model are consistent with the spine model in SAP2000.

The force-displacement laws to be assigned to the inelastic supports are calculated by using a by-hand pseudo-pushover analysis (described in subsection 4.1). Simple programming routines are developed in MATLAB [49] to apply the DBA approaches with very low modelling/computational effort.

3.3. Seismic action

The ground-motion record suite adopted to analyse the case-study bridges is described in this subsection. First, a suite of 20 natural spectrum-compatible ground-motion records is selected. The target spectrum is the normalised elastic response spectrum proposed by the EC8-part 1 [44] Type 1 for site class C (i.e. shear wave velocity $V_{s,30} = 180 - 360\ m/s$) scaled to a peak ground acceleration (a_g) of 0.50 g. It is used for the record selection carried out via the REXEL tool [50] by using the European Strong Motion Database [51] and the Selected Input Motions for displacement Based Assessment and Design database [52]. This tool is adopted to automatically select a suite of ground-motion records that are linearly scaled in amplitude to achieve compatibility with respect to the target spectrum within a given range of periods (Figure 4). In this case, this spectrum compatibility bandwidth is [0.15 s; 1.50 s], defined to include the elastic first-mode period of the analysed bridges and (a tentative value of) the period elongation associated with the stiffness degradation during the seismic response. The maximum adopted scale factor is equal to 3.5 avoiding large scaling which can produce not realistic scaled excitations. Finally, the entire suite of spectrum-compatible records and target spectrum is again scaled so that this latter reaches a_g equal to 0.20 g and 0.35 g. In this way, three suites of ground motions having a different seismic intensity are obtained.

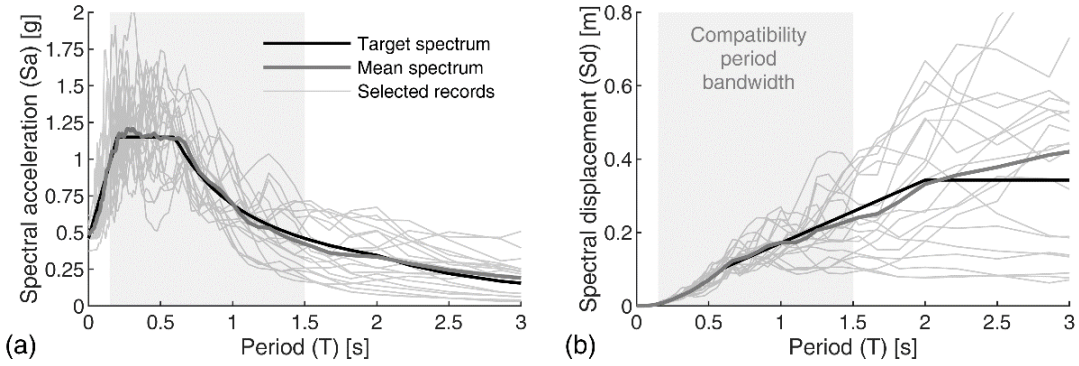

Figure 4. Target and mean 5%-damped spectra: (a) spectral accelerations and (b) displacements.

4. Seismic performance assessment of steel braced towers

This section focuses on the displacement-based performance assessment of isolated steel braced towers. The case-study towers are analysed by means of NLTHA, pushover analysis and a proposed simplified pseudo-pushover and the results are used to identify an accurate formulation for equivalent viscous damping. The outcomes of this section are used to solve the applicability issues of the direct DBA and CSM on steel truss bridges mentioned in Section 2.

4.1. Seismic analysis procedures

Pushover analyses and NLTHA are carried out by using the numerical models of the steel braced towers. For NLTHA, a tangent-stiffness damping strategy is selected and elastic damping equal to 3% is assigned to all the modal shapes. Additionally, a simplified analytical procedure is also used in this study to compare the pushover results and provide to the users a simple method based on by-hand calculations for achieving capacity curves of steel braced towers. This method does not resort to a nonlinear numerical model and can be applied with fast programming routines. The procedure mimics the steps of the pseudo-pushover analysis proposed by the New Zealand Society for Earthquake Engineering [53].

This simplified analysis approach is described in the flowchart shown in Figure 5. It is based on linear static analyses performed via an elastic two-dimensional model which is updated during the process. The adopted model represents the front of the tower composed of the legs (fully fixed to the foundations), the top beam, the horizontal and tensile diagonal braces (selected considering the pushing direction). The compression braces are neglected in the model, due to their low buckling load and fragile response. It is assumed that the seismic mass of the system is equal to the tributary seismic mass of the superstructure and it is lumped at the top of the tower.

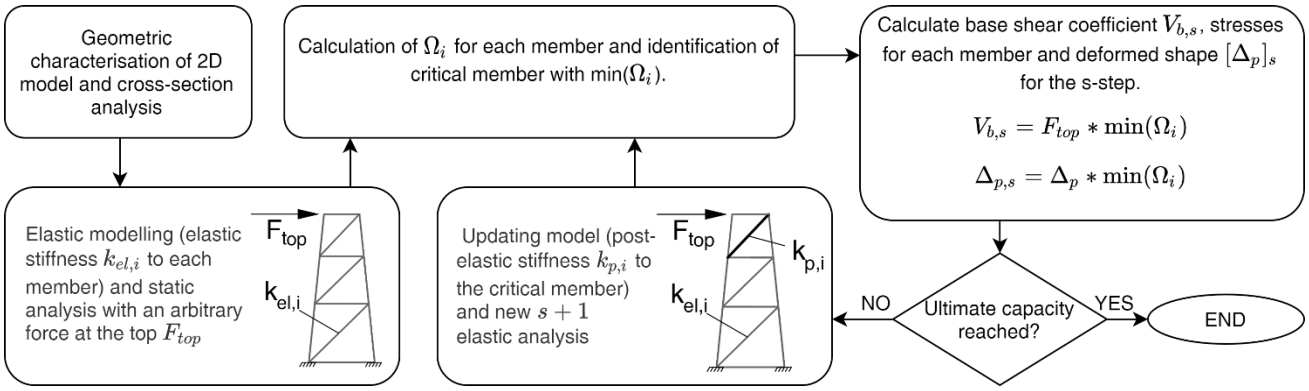

Figure 5. Flowchart of the analytical pseudo-pushover for steel braced towers.

First, the elastic stiffness is assigned to the different members of the model. A static analysis is performed with a force of arbitrary intensity placed at the top node of the tower. To consider the effect of the eccentricity of the seismic mass of the superstructure with respect to the top node of the tower (which can be relevant for analysis in transverse direction [54]), the force can be coupled with a moment equal to the force multiplied by the distance between the top of the tower and the superstructure cross-section centroid. A tributary portion of the gravity loads is directly assigned to each leg as axial stress. The axial/flexural stress of each member is registered and compared to the corresponding capacity computing a strength-based capacity-demand ratio Ω_i for each *i-th* member. For the braces, Ω_i considers the axial stress only, while, for the legs, the axial-flexural interaction is accounted for by using the strength domain (see subsection 3.2). The displacement profile of the tower, which corresponds to the top displacement of each panel (Δ_p), is extracted. The member characterised by the minimum of the calculated Ω_i is assumed to reach the yielding at the considered load step. The total base shear $V_{b,s}$ and $\Delta_{p,s}$ at this *s-th* step are calculated by multiplying the counterpart provided by the static analysis for the minimum of the Ω_i ratios. If the ultimate capacity of the tower is reached (see Section 4.2), the analysis stops. If not, another *(s+1)-th* step is performed. In this case, the model is updated, assigning to the critical member its post-elastic stiffness and a new static analysis is performed. The newly calculated stresses are added to the ones calculated in the previous step; a new critical element is identified and another value of $V_{b,s+1}$ and $\Delta_{p,(s+1)}$ is achieved.

4.2. Capacity curves and damage states

Figure 6 shows the capacity curves for the steel braced towers (named T1 and T2) calculated via the previously described strategies. The DS thresholds are represented in Figure 7 to understand the sequence of seismic damage which induces a nonlinear ductile/fragile response of the analysed steel braced towers. Three DS thresholds based on the local nonlinear response of the steel members (Table 1) are identified on the obtained capacity curves following the recommendations of the guidelines in Ref. [21]. The DS1 corresponds to minimal post-earthquake damages which can be repaired without affecting the bridge serviceability. The DS2 includes repairable damages, not affecting the gravity load safety of the tower which, also, keeps an adequate residual capacity to seismic loading. The DS3 reflects a near-collapse condition, accounting for fragile failure modes and severe damages on steel members. For DS3, the repairing interventions can require large efforts in terms of time and cost. As shown in Table 1, the axial buckling of the horizontal braces is supposed to imply a fragile response. Indeed, it can induce an important stress redistribution leading to a loss of global tower strength and can lead to a large increase in the effective length of the legs reducing the safety in terms of leg global buckling (considering that the buckling load of the diagonal braces is very prematurely reached).

Figure 6 shows that the consistency between numerical and pseudo-pushover approaches is satisfying, proving the validity of the assumptions of the simplified method. The capacity curves related to the longitudinal direction (i.e. longitudinal axis of the bridge) show a ductile response: the yielding of the (at least one) tensile diagonal braces (which determines the DS1) anticipates the nonlinear response of the legs. The plastic rotation at the top of the legs determines the reaching of DS2. No shear failure is detected. The DS3 corresponds to the reaching of the ultimate plastic rotation at the top of the legs. On the other hand, a fragile response is observed in the transverse direction, where the axial buckling of the horizontal braces induces the reaching of a near-collapse DS3, anticipating other ductile failure modes. This is because of the increased length of the horizontal braces with respect to the longitudinal direction, which reduces the corresponding critical buckling load. The large strength degradation involved by the failure of horizontal braces is shown in Figure 6 as a dotted line.

To study the nonlinear response of the towers in the transverse direction in the following sections, a retrofitted version of the steel braced towers is introduced. The cross-section area of the horizontal braces is increased until a ductile response of the tower is activated, simulating a retrofit intervention aimed at increasing their critical buckling load. The capacity curves in Figure 6 for the retrofitted cases show that the hierarchy of strength is consistent with the one observed in the longitudinal direction.

Table 1. Damage state description of steel braced towers.

Damage State	Description
DS1	Yielding of the tensile diagonal braces (minimal damages, $\mu_d = 1$) Flexural yielding of the legs or top beams (minimal damages, $\mu_l = 1$)
DS2	Large plastic rotation of the legs or top beams (repairable damages, $\mu_l = 1.5$)
DS3	Ultimate flexural ductility on legs or top beams (severe damage, $\mu_l = 2$) Buckling of a longitudinal profile of the battened legs Shear failure of the legs Axial buckling of horizontal braces

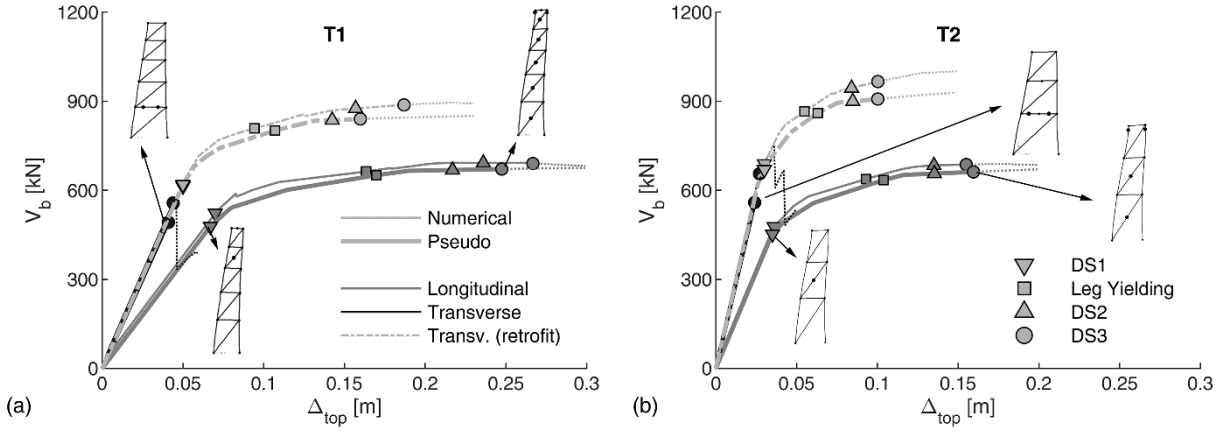

Figure 6. Capacity curves and pseudo-pushover curves of the case-study steel braced towers: a) T1 tower; b) T2 tower .

4.3. Equivalent viscous damping strategies for simplified seismic performance assessment

Equivalent viscous damping coefficients ξ_{eff} are used within the DBA approaches (subsection 2.1) and the CSM (subsection 2.2) simulating the energy dissipation capacity of an inelastic structure/structural member subjected to cyclic action. It is equal to the sum of the elastic ξ_{el} and hysteretic ξ_{hyst} damping. For steel structures ξ_{el} is generally equal to 0.02-0.03 [55]. Several formulations for computing ξ_{hyst} calibrated for different structural typologies are proposed in the literature (e.g. [17]), but no recommendations are explicitly reported for steel braced towers.

The steel braced towers can be studied as concentrically braced multi-storey structural systems with slender diagonal braces arranged in different panels. It can be reasonably assumed that the main source of hysteretic dissipation is associated with the nonlinear response of the diagonal braces which are subjected to axial buckling in compression and yielding in tension [56]. Figure 6 confirms this assumption showing that, in the case of ductile behaviour, the nonlinear response is activated by the yielding of tensile steel braces only. The dissipation of the legs can be neglected with respect to the dissipation of the diagonal braces since the amount of seismic force absorbed by the legs is negligible compared to the portion absorbed by the diagonal

braces. Furthermore, this source of dissipation can not be modelled using the lumped-plasticity modelling strategy adopted which considers axial load-flexure interaction.

Considering the similarity with respect to multi-storey steel concentrically braced frames, the equivalent viscous damping related to the tower ξ_{tow} is computed aggregating the elastic and the hysteretic dissipation of the braced panels according to the approach proposed by Grande & Rasulo [56]. This latter is tailored for steel braced towers in Equation (8) using the equivalent viscous damping of the specific panel $\xi_{hyst,p}$, the yielding steel strength f_y, the cross-section area of the tensile diagonal brace $A_{d,p}$ and its axial deformation ε_p, the top displacement Δ_{top} and the total base shear V_b of the tower.

$$\xi_{tow} = \xi_{el} + \xi_{hyst} = 0.03 + \frac{\sum_{p=1}^{N} \xi_{hyst,p} f_y A_{d,p} \varepsilon_p}{\Delta_{top} V_b} \tag{8}$$

The precursor approach for estimating ξ_{hyst} of an inelastic system is the area-based approach proposed in the study by Jacobsen [57] (and quoted by Priestley et al. [17]) about substitute-structure analysis. The ξ_{hyst} to be assigned to the substitute structure having linear behaviour and secant-stiffness in target displacement condition is proportional to the energy absorbed during a hysteretic steady-state cycle at the given target displacement by the investigated structure. This approach establishes that ξ_{hyst} can be calculated according to Equation (9) where A_h is the area measured in a steady-state cycle, V_m and Δ_m are the maximum force and the target displacement. Goggins et al. [58] proposed a displacement-based design methodology for concentrically braced frame systems. They compared the ξ_{hyst} calculated with the area-based approach based on experimental test results on a concentrically braced panel, to literature ξ_{hyst} formulations. They stated that the formulation by Priestley et al. [17] related to a Flag-Shaped ($\beta = 0.35$) hysteresis response (Equation (10), where $C_{evd} = 0.186$ and μ is the ductility demand of the structure) is consistent to the experimental area-based ξ_{hyst} considering a steady-state response. However, a strong overestimation of the displacement demand was detected after comparisons with shake table tests using real records. The authors recommended to adopt the Takeda-Thin formulation by Priestley et al. [17] (Equation (10) where $C_{evd} = 0.444$) for calculating the ξ_{hyst} of concentrically-braced structures in displacement-based design applications. This result is consistent with the displacement-based design approach by Della Corte & Mazzolani [59].

$$\xi_{hyst} = \frac{A_h}{2\pi V_m \Delta_m} \tag{9}$$

$$\xi_{hyst} = C_{evd} \frac{\mu - 1}{\pi \mu} \tag{10}$$

Besides these studies, Wijesundara et al. [55] proposed formulations to calculate ξ_{hyst} for displacement-based design applications of concentrically-braced steel frames. The authors calculated the ξ_{hyst} according to the area-based approach and performed additional calibrations based on NLTHA using natural ground motions. They calibrated ξ_{hyst} for varying ductility (μ_P from 1 to 7) and non-dimensional slenderness ratio (λ_P from 0.41 to 0.83) of the diagonal brace of a single panel and proposed a final synthetic analytical equation. However, the proposed equation is not applicable for very high values of the slenderness of the bracing systems which characterise the structural typology analysed in this study.

According to this state-of-the-art description, some strategies are selected and analysed in this study to approximate the hysteretic dissipation of the single braced panel of the steel towers $\xi_{hyst,p}$. The first follows the fundamentals of the area-based approach by Jacobsen [57] (indicated as JB). Several case-study panels having parametric non-dimensional slenderness of diagonal braces are subjected to cyclic pushover analysis to calculate the steady-state response. The $\xi_{hyst,p}$ is calculated according to Equation (9) for Δ_m equal to [2.5, 3.5, 4.5, 5.5], corresponding to μ_P equal to [1.5, 2, 2.5, 3, 5, 6.5, 8]. Nonlinear regression with a surface model is performed via the least square method to achieve the synthetic Equation (11) relating the $\xi_{hyst,p}$ to μ_P and λ_p. The process is described in Figure 7. The second strategy (indicated as CBF) considers the outcomes of the study by Wijesundara et al. [55]. The calibrated equivalent viscous damping data which refers to the braced panels with coupled diagonals in Ref. [55] are adopted to fit another nonlinear model via the least square method. The model is proposed in Equation (12). The dependency on λ_P is neglected in this case. The third (TT) and fourth (FS) strategies refer to Equation (10) using C_{evd} equal to 0.444 and 0.186.

$$\xi_{hyst,p} = \left(\lambda_p^{0.132} - 1\right)\frac{\mu_p - 1}{\mu_p^{1.5} + 0.5} \tag{11}$$

$$\xi_{hyst,p} = 0.218\,\frac{\mu_p - 1}{\mu_p - 0.76} \tag{12}$$

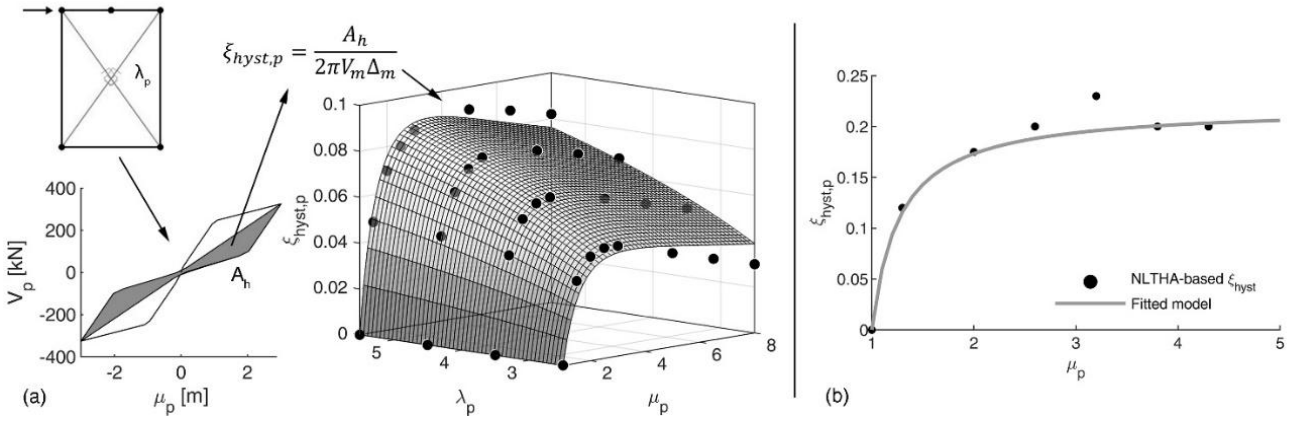

Figure 7. (a) Strategy for calculating area-based equivalent viscous damping and fitting of the surface model; (b) fitting of NLTHA-based equivalent viscous damping by Wijesundara et al. [55].

4.4. Effectiveness of the selected strategies for equivalent viscous damping

The accuracy of the candidate equivalent viscous damping formulations selected in the literature is evaluated in this section. For this purpose, the capacity curves calculated in subsection 4.2 are subjected to the CSM by using the candidate equivalent viscous damping formulations to calculate the performance displacement. The best estimate with respect to NLTHA determines the "best" strategy. The smooth code-based spectra are used within the CSM, while the average displacement obtained by using the 20 records associated with each ground-motion suite is the NLTHA result. To apply the CSM, the capacity curves are converted in SDoF capacity spectra (relating the acceleration-displacement response of an equivalent SDoF system of the tower). The acceleration is obtained by dividing the base shear for the effective mass of the tower approximated as the tributary seismic mass of the superstructure placed at the top node of the tower. The mass of the tower itself is neglected since it is about 1/20 of the superstructure mass [6]. Accordingly, the equivalent SDoF displacement can be also approximated as the displacement registered at the top node of the tower where the mass is lumped. Note that to consider the real distribution of seismic mass of the tower in calculating the SDoF capacity spectra, the equivalent SDoF displacement and the effective mass can be calculated via Equations (2) and (3).

Figure 8a provides a preliminary comparison among the ξ_{tow} values calculated via the selected strategies. It is observed that the FS and JB strategies strongly underestimate the ξ_{tow} with respect to the other strategies ($\xi_{tow} \cong 0.07$ at $\Delta_{top} = 0.20m$), the CBF provides the maximum value of ξ_{tow} (equal to 0.15 at $\Delta_{top} = 0.20m$), while TT provides intermediate estimations (ξ_{tow}=0.10 at $\Delta_{top} = 0.20m$).

The relative errors calculated between the results of the CSM applied using the candidate equivalent viscous damping formulations and the NLTHA are graphically reported in Figure 8b. The errors are calculated for the T1 and T2 towers, analysed in both longitudinal and transverse direction by using numerical and pseudo- pushover procedures. The outcomes are particularly consistent with the literature studies mentioned in subsection 4.3. Indeed, the FS and JB formulations are too conservative and provide a large overestimation with respect to the NLTHA. The errors increase as the intensity of the seismic action increases. This evidences the need for NLTHA-based calibration for equivalent viscous damping based on steady-state cyclic analysis. The TT formulation provides errors between [+15;+52]% endorsing the findings of Della Corte & Mazzolani [59]. The strategy CBF outperforms the other approaches providing errors generally lower than +10%. The maximum error is equal to +23% and +21% corresponding to the T2 analysed in longitudinal direction via numerical pushover and pseudo-pushover, respectively. It is worth noting that, in this case, the accuracy of this formulation seems to be not sensitive to the intensity of the seismic action and nonlinear demand.

These results suggest that the CBF formulation provide a satisfactory accuracy for the seismic performance assessment of the steel braced towers. These outcomes can be directly applied for the seismic performance assessment of isostatic steel truss bridges with steel braced towers similar to the analysed cases. Given these results, the CBF formulation is used to test the analysis procedures described in Section 2 for hyperstatic continuous-truss bridges in the following Section.

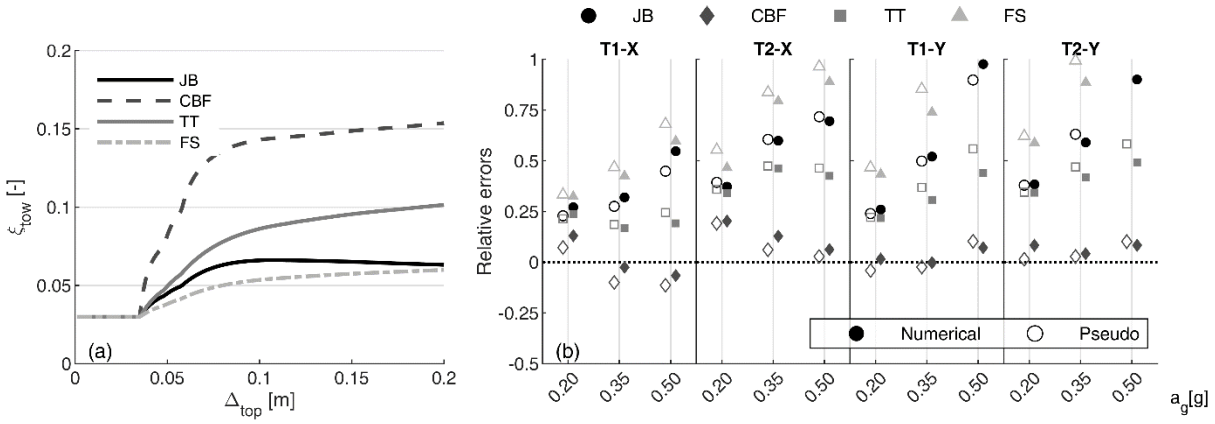

Figure 8. (a) Comparison of the equivalent viscous damping strategies for T2 tower (Y direction) using numerical pushover analysis. (b) Relative errors between the performance displacement calculated via the CSM adopting the candidate equivalent viscous damping strategies and NLTHA (X: longitudinal direction, Y: transverse direction).

5. Effectiveness of DBA and nonlinear static approaches for steel truss bridges

The results of the DBA and nonlinear static procedures (Section 2) are applied on parametric case-study bridges in this section. The bridges are analysed in the transverse direction only according to previous literature studies (e.g. [13,60]). To better interpret the final results, a preliminary discussion on the regularity of the seismic response of the analysed bridges is proposed. Then, the results are presented in terms of estimated performance displacement using the smooth code-based response spectra and fragility curves.

5.1. Parametric case-study bridges

A dataset of six case-study continuous-truss bridges is generated by using the geometric/constructive features of the archetype bridge (subsection 3.1). The case studies, shown in Figure 9, differ in the number of spans and geometric layout of the supporting steel towers. The length of the span is 42 m according to the archetype bridge. Each case study is identified by a code related to the identification number of the towers composing the substructure (e.g. B121 is a four-span bridge with two external T1 towers and a central T2 tower).

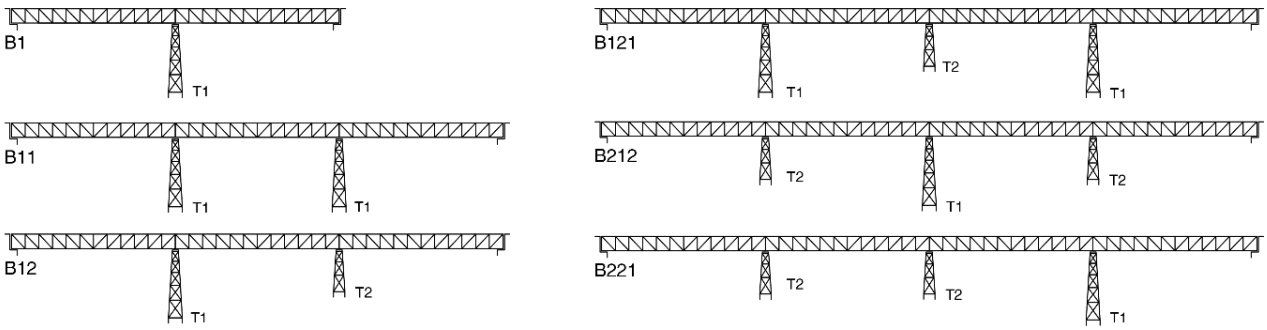

Figure 9. Parametric case-study steel truss bridges.

5.2. Modal analysis and relative stiffness index

According to several studies (e.g. [9,10,16,19,60]), the degree of regularity strongly influences the accuracy of simplified nonlinear static procedures and DBA approaches. Seismic regular response of continuous-superstructure bridges means: 1) low influence of higher modes in elastic state and 2) slight modifications of the significant modal shapes for increasing nonlinear demand [9]. The first-mode participating mass (considering the transverse direction) is calculated for the case-study bridges to evaluate the regularity condition 1), whereas for condition 2) the Relative Stiffness index (RS) [61] is introduced. This latter is calculated with Equation (13) and compares the stiffness in the transverse direction of the superstructure and

supporting towers. As shown by Gentile et al. [19], the higher is the RS, the higher is the influence of the superstructure in redistributing the seismic action among the substructure members, reducing the variability of the modal shapes for increasing inelastic demands.

$$RS = \frac{384EJ_{sup}}{5L_{sup}^3} \Big/ \sum k_{tow} \tag{13}$$

The results of the modal analysis are shown in Figure 10. All the modal shapes characterised by a participating mass M^* higher than 5% are shown. The RS index is also indicated in the titles of the subfigures. Figure 10 shows that, for all the analysed bridges, the first-mode periods ranging between 0.72 s and 0.65 s are similar to the vibration period of the T1 tower (equal to 0.65 s) and the first modal shape is associated with the dynamic excitation of the T1 tower which is more flexible than T2. The participating mass of the first mode M_1^* increases according to the ratio between the tributary seismic mass of the T1 towers and the total seismic mass. Indeed, the first modal shapes of the B1, B11 and B121 bridges correspond to M_1^* higher than 80%. Conversely, the modal shapes of the B12, B212 and B221 bridges are affected by the high stiffness of short towers and, thus, are characterised by M_1^* equal to 0.62, 0.52 and 0.41, respectively. Figure 10d, e and f illustrate the strong differences in modal shapes and M_1^* for the analysed four-span bridges which result very sensitive to the stiffness distribution of the towers along the bridge longitudinal axis. For these cases, the substructure members govern the seismic response rather than the superstructure. Opposite results are related to the study by Gentile et al. [19] that registered $M_1^* \geq 0.70$ for ordinary RC case-study bridges (two- to six-spans) regardless of the substructure layout.

Furthermore, the observed RS indexes are much lower with respect to the RS calculated by Gentile et al. [19] for RC continuous-deck bridges. This proves that the superstructure influence in redistributing the inertia forces on substructure components is much lower in continuous-deck steel truss with respect to the wide-spread RC bridges. For example, the RS indexes related to the analysed four-span steel truss bridges are equal to 0.0084 and 0.0068 and lower than the RS registered for six-span continuous-deck RC bridges in Ref. [19] which is higher than 0.035. According to these differences, it can be claimed that, although DBA and nonlinear static procedures are widely validated for RC continuous-deck bridges, specific tests are needed for use with steel truss bridges.

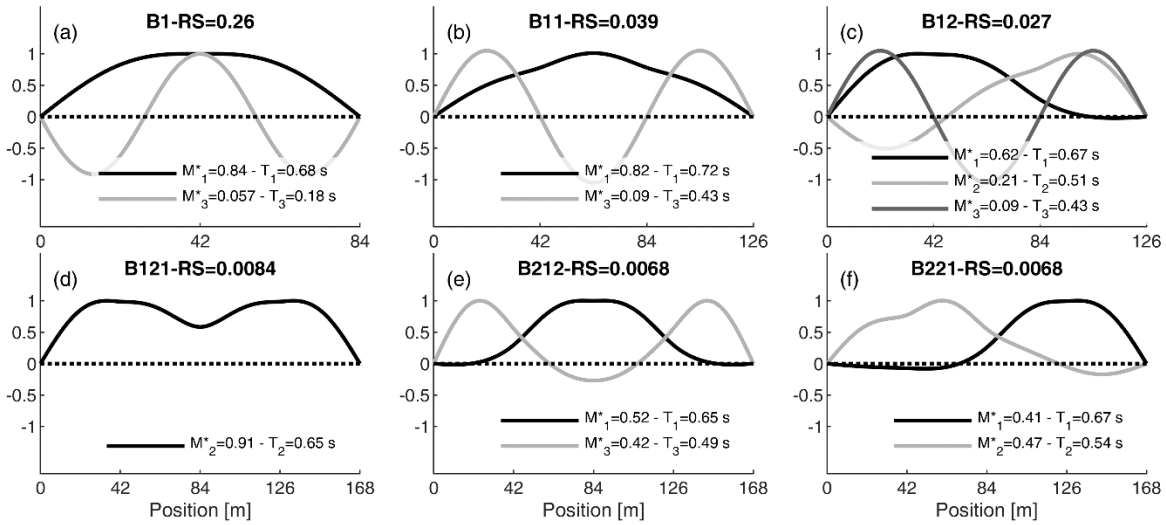

Figure 10. Significant modal shapes (participating mass M^* higher than 5%) and RS of the parametric case-study bridges.

5.3. Accuracy in performance displacement evaluation

This subsection deals with the accuracy of the considered DBA (IEMS, ITERSA and S-IRSA) and nonlinear static procedures (PUSHm and PUSHu coupled with the CSM) for a deterministic seismic assessment using the smooth code-based response spectra presented in subsection 3.3. The NLTHA is performed by using the three suites of 20 scaled records and the average displacement demand is extracted to benchmark the simplified analysis approaches.

The capacity-demand ratio (CDR) and bridge index (BI) are introduced to compare the obtained results. The CDR measures the accuracy of all the simplified approaches with respect to NLTHA in predicting the performance of the critical supporting tower with respect to the DS3. It is calculated via Equation (14) where t indicates each tower of the analysed bridge and N_t the total number of supporting towers. Note that the ultimate displacement capacity $\Delta_{U,t}$ assumed in the DBA approaches differs with respect to the one assumed in numerical procedures. Indeed, $\Delta_{U,t}$ is calculated through the simplified pseudo-pushover within the DBA, while for both the global numerical pushover and NLTHA, the $\Delta_{U,t}$ provided by the numerical pushover is adopted. Furthermore, the BI (Equation (15)) evaluates the accuracy of each simplified analysis approach in predicting the whole performance displacement profile with respect to NLTHA. The BI herein adopted is a modified version with respect to the one proposed by Gentile et al. [19] and Pinho et al. [60] and measures the average relative errors on the target displacement profile predicted by the simplified approaches with respect to NLTHA.

$$CDR = \min_{t=1}^{N_t}\left(\frac{\Delta_{U,t}}{\Delta_t}\right) \tag{14}$$

$$BI = \frac{1}{N_t}\sum_{t=1}^{N_t}\left|\frac{\Delta_t^{DBA/PUSH}}{\Delta_t^{NLTHA}} - 1\right| \tag{15}$$

Figure 11a shows the relative errors on the CDR calculated via the DBA and nonlinear static procedures with respect to NLTHA, while the BIs are reported in Figure 11b. To better understand these results, the performance displacement predicted by the considered analysis approaches for each mass node on the superstructure is shown in Figure 12 (a spline interpolation is used to simulate the displacement between adjacent nodes). Moreover, the standard deviation of the displacement demand predicted by the NLTHA is also shown. For the B1, B11 and B121 cases, the ITERSA and IEMS coincide since higher-mode contributions are negligible in both elastic and inelastic phases. For the B1 and B11 cases, all the DBA and nonlinear static procedures exhibit a general accuracy. Indeed, the corresponding relative errors on the CDR with respect to NLTHA is included in the range [-21; 0]% and the BIs are lower than 15%. For both these case studies, the DBA approaches underestimate the CDRs with respect to NLTHA. This effect is caused by an underestimation of the ultimate capacity on the T1 tower provided by the simplified pseudo-pushover (Figure 6). For the B121 bridge, the IEMS and ITERSA provide errors on CDR lower than -23% and BIs higher than 20% for a_g equal to 0.35g. This is explained by Figure 12d which shows that these strategies fail in predicting the performance displacement profile, overestimating the demand of the central tower and underestimating it on the lateral towers. This is because the adopted algorithm based on secant-to-target-displacement stiffness updates the deformed profile non-consistently with respect to NLTHA after the first yielding of the central tower. On the other hand, the S-IRSA, which neglects the updating of modal shapes and use the secant-to-yielding stiffness only, outperforms the other DBA approaches regardless of the seismic intensity. The PUSHu offers a satisfying accuracy for the B1, B11 and B121 bridges, while the PUSHm leads to errors on CDR higher than 20% for B121 and the considered medium- and high-intensity levels of a_g.

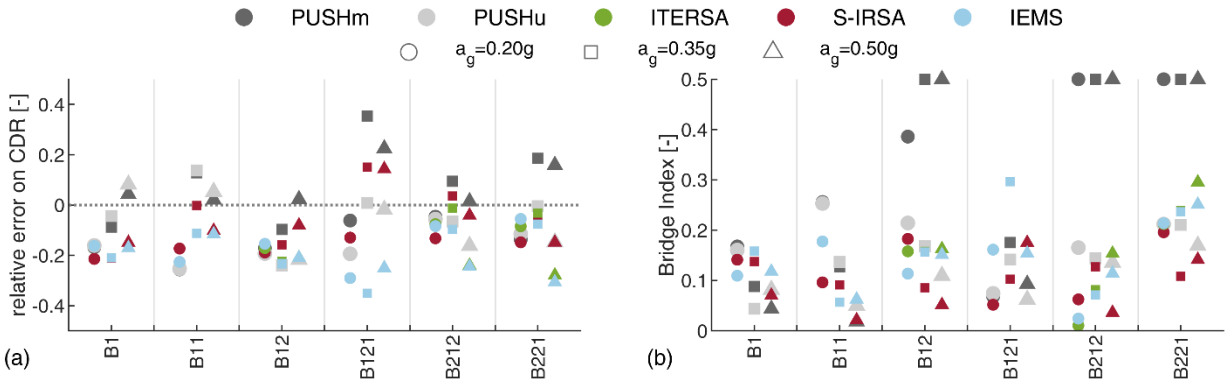

Figure 11. Relative errors on the CDR (a) and BI (b) for the case-study bridges.

The accuracy of the PUSHm importantly decreases for the B12, B212 and B221 where the higher-mode contribution is relevant (Figure 12d, e and f). It well predicts the target displacement of the T1 towers which is related to the first modal shape of the bridge underestimating the displacement demand on the shortest supporting T2 towers. Therefore, the BIs of PUSHm exceed 40% in these cases. The ITERSA and IEMS outperform the PUSHm because of the consideration of higher-mode contributions. Generally, these strategies accurately predict the NLTHA displacement demand leading to BIs mainly lower than 20%. ITERSA and IEMS are less accurate for increasing the inelastic demand, overestimating the displacement demand on the T1 towers associated with the first mode. For example, for the B221 and a_g equal to 0.50g, these strategies provide BIs equal to 25% and 30% and maximum errors on the CDRs equal to -28 and -30%, respectively. These errors can be again associated with the inaccuracies in updating the modal shapes within the iterations aimed at reaching the convergence on the secant-to-target-displacement stiffness. Indeed, the S-IRSA outperforms the other DBA strategies providing CDR-based errors and BIs lower than 20%. No substantial improvements in seismic performance assessment are registered in these cases by using the more refined ITERSA with respect to the simpler IEMS. The PUSHu, thanks to its tendency to envelope the contribution of higher modes with a uniform load profile, outperforms the PUSHm. Particularly, the corresponding error on the CDR is generally lower than 20%, while the BIs are included in the range [5; 22]%.

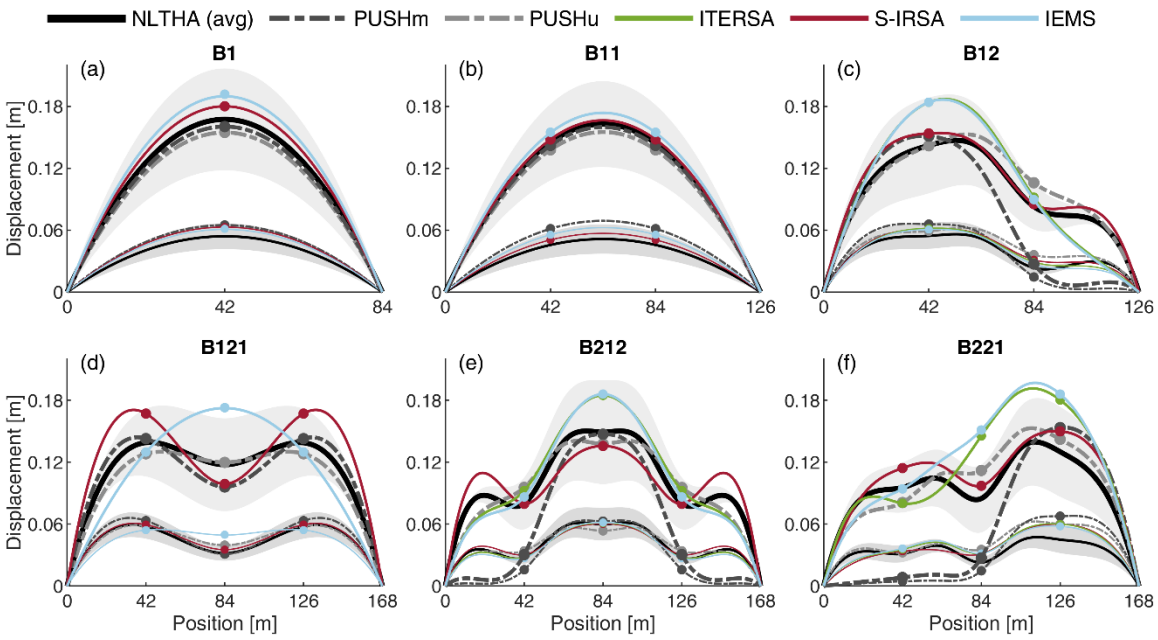

Figure 12. Displacement profiles calculated via pushover (PUSHm and PUSHu), DBA (ITERSA, IEMS, S-IRSA) procedures and NLTHA for a_g equal to $0.20g$ and $0.50g$.

In summary, the outcomes of this section show that the investigated nonlinear static and direct DBA methodologies provide a satisfying accuracy for the seismic performance assessment of multi-span steel truss bridges with a continuous superstructure provided that appropriate algorithms are used. Unlike other bridge typologies [13,19], the use of secant-to-target-displacement stiffness within DBA approaches can be inaccurate (i.e. ITERSA and IEMS). Therefore, the "non-adaptive" S-IRSA, which uses secant-to-yielding stiffness (i.e. elastic modal shapes), is recommended for bridges similar to the analysed case studies. Moreover, with reference to numerical pushover procedures, a uniform load pattern should be preferred to a first-mode-proportional one, to envelope higher-mode contributions. It is expected that these results can be extended also for other bridge types having high flexibility of the continuous superstructure, such as truss bridges supported by masonry/RC wall piers.

5.4. Accuracy in fragility analysis

The accuracy of the investigated simplified approaches in performing probabilistic seismic assessment according to the procedure proposed in subsection 2.3 is hereafter discussed. The fragility analysis considers two limit conditions: the first is related to the reaching of a severe damage condition (DS3 in Table 1) of one of the supporting towers, the second refers to the serviceability DS considering the limits for superstructure transverse deformation suggested by Ref. [43] for railway bridges.

The fragility analysis is performed by analysing each bridge using three suites of 20 scaled ground-motion records (subsection 3.3) consistently with previous literature studies [40,62]. The record-specific a_g is used as IM. The EDPs are defined in terms of demand-capacity ratios. For the first fragility analysis, the EDP is the maximum between the ratio of Δ_t divided by $\Delta_{U,t}$ related to the towers (the reciprocal of the CDR in Equation (9)). For the serviceability fragility analysis, the EDP is the highest of the demand-capacity ratios calculated by using the maximum angular variation and minimum radius of curvature of the superstructure extracted for each analysis and divided by the limits proposed in [43] (speed range: $V \leq 120\ km/h$). Since demand-capacity ratios are used, in both the cases, edp_{DS} is equal to 1. It is worth mentioning that the use of the iterative DBA algorithms with real ground-motion spectra can be unstable [36]. In this study, the cases where lack of convergence is registered (eight cases out of 60) are excluded for the generation of the probabilistic seismic demand models. Since the IEMS and ITERSA provide similar results in terms of performance assessment (Figure 12), only the latter is used for calculating fragility curves.

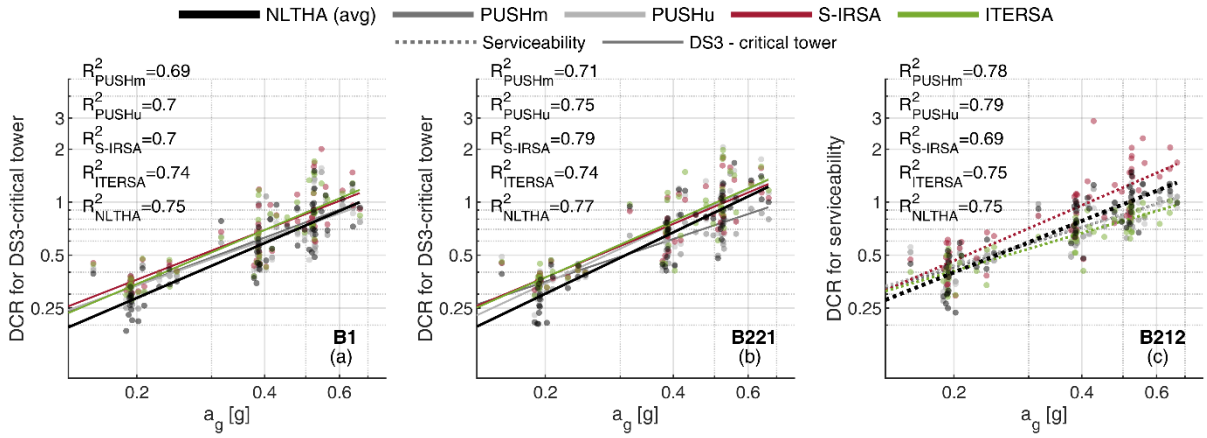

Figure 13. Probabilistic seismic demand model for B1 (a) and B221 (b) considering the DS3 of the critical tower, and for B212 (c) concerning bridge serviceability.

The probabilistic seismic demand models for three sample cases are reported in Figure 13, while the fragility curves for DS3 of the critical tower (continuous line pattern) and serviceability (dotted line pattern), related to the six case studies, are shown in Figure 14. The NLTHA-based fragility curves show that the serviceability DS anticipates the DS3 of the towers for these investigated case-study bridges. The fragility curves for DS3 of the critical tower approximately reflect the abovementioned results in terms of CDR (Figure 11a). Therefore, the DBA and nonlinear static approaches lead to satisfying accuracy. Indeed, the relative errors with respect to NLTHA on the median fragility (a_g related to a 50% exceedance probability) are generally

lower than 20% for S-IRSA and PUSHu. A lower accuracy of the investigated simplified approaches is registered for the PUSHm, leading to errors on the median fragility higher than +29% for the B212 and B221. The ITERSA underestimates (-27%) the NLTHA-based median fragility for the B121. The PUSHm provides a strong overestimation (+30%) of the NLTHA-based median fragility for the B221. Referring to the serviceability limit state, the effectiveness of the adopted approaches is related to the corresponding accuracy in predicting the maximum deformation of the superstructure approaching the abutments. The ITERSA strongly overestimates the median fragility with respect to NLTHA for the B121 and B212 bridges, reflecting the inaccuracies in the deformed shape prediction shown in Figure 12d (errors on the median higher than 100% and equal to 37%, respectively). The other approaches generally provide higher accuracy with relative errors on median fragility lower than 20% with respect to the NLTHA results. Despite the promising results, further investigations should be performed on the effectiveness of the investigated simplified approaches for fragility analysis. Indeed, their accuracy could be sensitive to factors such as the adopted IM, the EDP or the input ground-motion suite. Moreover, to definitely assess the suitability of these approaches for bridge portfolio seismic assessment, the influence of the inaccuracies on fragility analysis should be evaluated with reference to the calculation of seismic risk metrics.

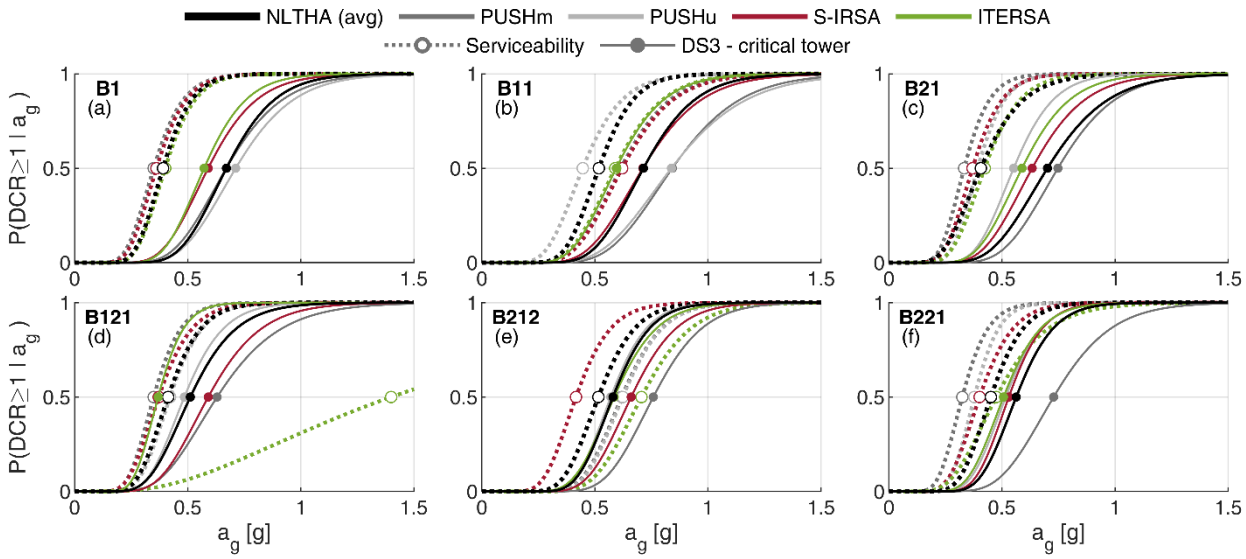

Figure 14. Fragility curves calculated via pushover (PUSHm and PUSHu), direct DBA (ITERSA and S-IRSA) procedures and NLTHA.

6. Conclusion

This study discusses the applicability and effectiveness of direct displacement-based assessment (DBA) and nonlinear static procedures for the seismic performance analysis of multi-span steel truss railway bridges with steel braced towers. An existing case-study historical European steel truss railway bridge is used as an archetype structure.

The first discussion presented in this study addresses some applicability issues of DBA or nonlinear static procedures concerning steel truss bridges, as opposed to widely analysed "conventional" RC bridges. A simplified pseudo-pushover procedure to compute force-displacement relationships of steel braced towers is proposed. Its accuracy is proved through comparison with numerical pushover analysis. Moreover, an equivalent viscous damping formulation to simulate the hysteretic response of steel braced towers is identified among several literature-based candidates. The proposed formulation, used within the capacity spectrum method, provides errors lower than 20% with reference to nonlinear time-history analysis (NLTHA) for the analysed case-study steel towers.

The second discussion evaluates the effectiveness of novel and state-of-the-art DBA algorithms considering higher-mode contributions and numerical pushover analyses coupled with the capacity spectrum method for the seismic performance analysis of continuous-superstructure steel truss bridges. Six case-study bridges with different substructure layouts and number of spans, generated by using the archetype structure, are analysed via three ground-motion suites having different intensity levels. It is observed that the investigated DBA approaches, thanks to the consideration of higher modes, can accurately be applied for the deterministic seismic assessment in terms of displacement demand on the critical tower and bridge performance displacement profile (i.e. errors generally lower than 20% with respect to NLTHA). The DBA approaches can be less accurate if the modal shapes are updated based on the secant-to-target-displacement stiffness of the substructure members. Also, uniform-load nonlinear static procedures provide a satisfying accuracy for the seismic performance assessment of this bridge typology. The accuracy of the investigated simplified methodologies is also reflected in the probabilistic seismic assessment considering the severe damage of the supporting towers and limits of superstructure transverse deformation.

This study is deemed to extend the current state-of-the-art research, which includes poor results on the seismic performance or fragility assessment of steel truss railway bridges. The findings achieved can be used for the seismic risk assessment of bridge portfolios including the investigated bridge typology. Further developments can be addressed to extend the proposed simplified procedures for the calculation of risk metrics (e.g. financial losses, expected network downtime) which can be directly used for modelling the vulnerability of transport networks or resilience analysis of populated contexts.

7. List of abbreviations

BI	bridge index	IM	intensity measure
CDR	capacity demand ratio	NLTHA	nonlinear time-history analysis
CSM	capacity spectrum method	PUSHm	first-mode-load pushover analysis
DBA	displacement	PUSHu	uniform-load pushover analysis
DS	damage state	RC	reinforced concrete
EDP	engineering demand parameter	RS	relative stiffness index
ITERSA	iterative response spectrum analysis	SDoF	single-degree-of-freedom
IEMS	iterative effective mode shape	S-IRSA	simplified iterative response spectrum analysis

8. Acknowledgements

This study was part of the Industrial PhD research program (PON-RI 2014-2020) sponsored by the Italian Ministry of University and Research (DOT130UZWT). We would like to express our gratitude to FGV (Ferrocarrils de la Generalitat Valenciana) and CALSENS S.L. for providing data of a real bridge, also to Juan Antonio García Cerezo, of FGV, for his invaluable cooperation and recommendations.

9. References

[1] Transforming our World: The 2030 Agenda for Sustainable Development (A/RES/70/1) 2015.

[2] Nations U. Sendai Framework for Disaster Risk Reduction 2015–2030 2015.

[3] Deng L, Wang W, Yu Y. State-of-the-Art Review on the Causes and Mechanisms of Bridge Collapse. J Perform Constr Facil 2016. https://doi.org/10.1061/(asce)cf.1943-5509.0000731.

[4] Leech T. The collapse of the Kinzua Viaduct. Am Sci 2005. https://doi.org/10.1511/2005.54.971.

[5] Silva V, Akkar S, Baker J, Bazzurro P, Castro JM, Crowley H, et al. Current challenges and future trends in analytical fragility and vulnerability modeling. Earthq Spectra 2019. https://doi.org/10.1193/042418EQS101O.

[6] Cardone D. Displacement limits and performance displacement profiles in support of direct displacement-based seismic assessment of bridges. Earthq Eng Struct Dyn 2014. https://doi.org/10.1002/eqe.2396.

[7] Stefanidou SP, Kappos AJ. Methodology for the development of bridge-specific fragility curves. Earthq Eng Struct Dyn 2017;46:73–93. https://doi.org/10.1002/eqe.2774.

[8] Şadan OB, Petrini L, Calvi GM. Direct displacement-based seismic assessment procedure for multi-span reinforced

concrete bridges with single-column piers. Earthq Eng Struct Dyn 2013. https://doi.org/10.1002/eqe.2257.

[9] Isakovic T. Higher modes in simpliÿed inelastic seismic analysis of single column bent viaducts 2006:95–114. https://doi.org/10.1002/eqe.535.

[10] Isaković T, Nino Lazaro MP, Fischinger M. Applicability of pushover methods for the seismic analysis of single-column bent viaducts. Earthq Eng Struct Dyn 2008;37:1185–202. https://doi.org/10.1002/eqe.813.

[11] Paraskeva TS, Kappos AJ, Sextos AG. Extension of modal pushover analysis to seismic assessment of bridges. Earthq Eng Struct Dyn 2006;35:1269–93. https://doi.org/10.1002/eqe.582.

[12] Paraskeva TS, Kappos AJ. Further development of a multimodal pushover analysis procedure for seismic assessment of bridges. Earthq Eng Struct Dyn 2010;39:211–22. https://doi.org/10.1002/eqe.947.

[13] Perdomo C, Monteiro R. Extension of displacement-based simplified procedures to the seismic loss assessment of multi-span RC bridges. Earthq Eng Struct Dyn 2020. https://doi.org/10.1002/eqe.3389.

[14] Pinho R, Monteiro R, Casarotti C, Delgado R. Assessment of continuous span bridges through nonlinear static procedures. Earthq Spectra 2009;25:143–59. https://doi.org/10.1193/1.3050449.

[15] Perdomo C, Monteiro R, Sucuoğlu H. Generalized force vectors for multi-mode pushover analysis of bridges. Bull Earthq Eng 2017;15:5247–80. https://doi.org/10.1007/s10518-017-0179-6.

[16] Kohrangi M, Bento R, Lopes M. Seismic performance of irregular bridges – comparison of different nonlinear static procedures. Struct Infrastruct Eng 2015;11:1632–50. https://doi.org/10.1080/15732479.2014.983938.

[17] Priestley MJN, Calvi GM, Kowalsky MJ. Displacement-based seismic design of structures. IUSS Press, Pavia, Italy; 2007.

[18] Cademartori M, Sullivan TJ, Osmani S. Displacement - based assessment of typical Italian RC bridges. Bull Earthq Eng 2020. https://doi.org/10.1007/s10518-020-00861-9.

[19] Gentile R, Nettis A, Raffaele D. Effectiveness of the Displacement-Based seismic performance Assessment for continuous RC bridges and proposed extensions. Eng Struct 2020. https://doi.org/10.1016/j.engstruct.2020.110910.

[20] Pipinato A. Extending the lifetime of steel truss bridges by cost-efficient strengthening interventions. Struct Infrastruct Eng 2018;14:1611–27. https://doi.org/10.1080/15732479.2018.1465103.

[21] MCEER. Seismic retrofitting guidelines for complex steel truss highway bridges. Multidisciplinary Center for

Earthquake Engineering Research State University of New York at Buffalo, Federal Highway Administration; 2006.

[22] Pipinato A, Pellegrino C, Bursi OS, Modena C. High-cycle fatigue behavior of riveted connections for railway metal bridges. J Constr Steel Res 2009;65:2167–75. https://doi.org/10.1016/j.jcsr.2009.06.019.

[23] Pipinato A, Pellegrino C, Modena C. Fatigue assessment of highway steel bridges in presence of seismic loading. Eng Struct 2011;33:202–9. https://doi.org/10.1016/j.engstruct.2010.10.008.

[24] Silva ALL, Correia JAFO, Xin H, Lesiuk G, De Jesus AMP, Augusto Fernandes A, et al. Fatigue strength assessment of riveted details in railway metallic bridges. Eng Fail Anal 2021. https://doi.org/10.1016/j.engfailanal.2020.105120.

[25] Buitrago M, Bertolesi E, Calderón PA, Adam JM. Robustness of steel truss bridges: Laboratory testing of a full-scale 21-metre bridge span. Structures 2021. https://doi.org/10.1016/j.istruc.2020.12.005.

[26] Yilmaz MF, Çalayan B. Seismic assessment of a multi-span steel railway bridge in Turkey based on nonlinear time history. Nat Hazards Earth Syst Sci 2018;18:231–40. https://doi.org/10.5194/nhess-18-231-2018.

[27] Freeman SA. Development and use of capacity spectrum method. Proc. 6th U.S. Natl. Conf. Earthq. Engng., Seattle: CD-ROM, EERI, Oakland; 1998.

[28] Nettis A, Raffaele D, Uva G. SIMPLIFIED FRAGILITY ANALYSIS OF MULTI-SPAN ISOSTATIC RC-BRIDGES CONSIDERING AN INCOMPLETE KNOWLEDGE LEVEL. 8th Int. Conf. Comput. Methods Struct. Dyn. Earthq. Eng. Methods Struct. Dyn. Earthq. Eng., 2021. https://doi.org/10.7712/120121.8718.18736.

[29] Kowalsky MJ. A displacement-based approach for the seismic design of continuous concrete bridges. Earthq Eng Struct Dyn 2002;31:719–47. https://doi.org/10.1002/eqe.150.

[30] Lin Y-Y, Miranda E. Noniterative Equivalent Linear Method for Evaluation of Existing Structures. J Struct Eng 2008. https://doi.org/10.1061/(asce)0733-9445(2008)134:11(1685).

[31] Fajfar P, Gašperšič P. The N2 method for the seismic damage analysis of RC buildings. Earthq Eng Struct Dyn 1996. https://doi.org/10.1002/(SICI)1096-9845(199601)25:1<31::AID-EQE534>3.0.CO;2-V.

[32] CEN. Eurocode 8 (EN 1998-3: 2004) Design of structures for earthquake resistance—Part 3: Assessment and retrofitting of buildings. Brussels, Belgium: 2005.

[33] Freeman SA. Development and use of capacity spectrum method. Proc 6th US NCEE Conf Earthq Eng 1998.

[34] ATC. Applied Technology Council (ATC-40) - Seismic evaluation and retrofit of concrete buildings 1996.

[35] FEMA. Improvement of Nonlinear Static Seismic Analysis Procedures. FEMA 440, Fed Emerg Manag Agency, Washingt DC 2005.

[36] Nettis A, Gentile R, Raffaele D, Uva G, Galasso C. Cloud Capacity Spectrum Method: accounting for record-to-record variability in fragility analysis using nonlinear static procedures. Soil Dyn Earthq Eng 2021. https://doi.org/10.1016/j.soildyn.2021.106829.

[37] Bakalis K, Vamvatsikos D. Seismic Fragility Functions via Nonlinear Response History Analysis. J Struct Eng 2018. https://doi.org/10.1061/(asce)st.1943-541x.0002141.

[38] Cornell CA, Jalayer F, Hamburger RO, Foutch DA. Probabilistic basis for 2000 SAC federal emergency management agency steel moment frame guidelines. J Struct Eng 2002. https://doi.org/10.1061/(ASCE)0733-9445(2002)128:4(526).

[39] Jalayer F, Ebrahimian H, Miano A, Manfredi G, Sezen H. Analytical fragility assessment using unscaled ground motion records. Earthq Eng Struct Dyn 2017;46:2639–63. https://doi.org/10.1002/eqe.2922.

[40] Ruggieri S, Porco F, Uva G, Vamvatsikos D. Two frugal options to assess class fragility and seismic safety for low-rise reinforced concrete school buildings in Southern Italy. Bull Earthq Eng 2021. https://doi.org/10.1007/s10518-020-01033-5.

[41] Bertolesi E, Buitrago M, Adam JM, Calderón PA. Fatigue assessment of steel riveted railway bridges: Full-scale tests and analytical approach. J Constr Steel Res 2021. https://doi.org/10.1016/j.jcsr.2021.106664.

[42] Computer and Structures INC (CSI). SAP2000 - Structural Analysis Program 2018.

[43] EN. Eurocode - Basis of structural design - Annex A2: Application for bridges. 1990.

[44] CEN. Eurocode 3 (EN 1991-1-4) Design of steel structures - Part 1-1: General rules and rules for buildings. vol. 3. Brussels, Belgium: 2009. https://doi.org/10.1201/b18121-13.

[45] AISC. Specification for Structural Steel Buildings, ANSI / AISC 360-16. 2016.

[46] Lee K, Bruneau M. Seismic vulnerability evaluation of axially loaded steel built-up laced members II: Evaluations. Earthq Eng Eng Vib 2008. https://doi.org/10.1007/s11803-008-0832-9.

[47] Lee K, Bruneau M. Seismic vulnerability evaluation of axially loaded steel built-up laced members I: Experimental results. Earthq Eng Eng Vib 2008. https://doi.org/10.1007/s11803-008-0831-x.

[48] Georgiev TS, Zhelev DS, Raycheva LD. Performance assessment of concentrically braced frames with modified braces depending on the applied beam-column joints. COMPDYN 2017 - Proc. 6th Int. Conf. Comput. Methods Struct. Dyn. Earthq. Eng., 2017. https://doi.org/10.7712/120117.5459.17857.

[49] The MathWorks Inc. MATLAB . version 9.5.0.944444 (R2018b) 2018.

[50] Iervolino I, Galasso C, Cosenza E. REXEL: Computer aided record selection for code-based seismic structural analysis. Bull Earthq Eng 2010. https://doi.org/10.1007/s10518-009-9146-1.

[51] Ambraseys NN, Smit P, Douglas J, Margaris B, Sigbjörnsson R, Ólafsson S, et al. Internet site for European strong-motion data. Boll Di Geofis Teor Ed Appl 2004.

[52] Smerzini C, Galasso C, Iervolino I, Paolucci R. Ground motion record selection based on broadband spectral compatibility. Earthq Spectra 2014;30:1427–48. https://doi.org/10.1193/052312EQS197M.

[53] NZSEE. New Zealand Society for Earthquake Engineering - The seismic assessment of existing buildings - technical guidelines for engineering assessments 2017.

[54] Priestley MJN, Seible F, Calvi GM. Seismic design and retrofit of bridges. New York, USA: John Wiley and Sons; 1996.

[55] Wijesundara KK, Nascimbene R, Sullivan TJ. Equivalent viscous damping for steel concentrically braced frame structures. Bull Earthq Eng 2011;9:1535–58. https://doi.org/10.1007/s10518-011-9272-4.

[56] Grande E, Rasulo A. Seismic assessment of concentric X-braced steel frames. Eng Struct 2013;49:983–95. https://doi.org/10.1016/j.engstruct.2013.01.002.

[57] Jacobsen L. Damping in composite structures. Proc 2nd World Conf Earthq Eng 1960.

[58] Goggins JG, Sullivan TJ. Displacement-based seismic design of SDOF concentrically braced frames. Maz. Ricles, Sause STESSA 2009., Taylor & Francis Group; 2009.

[59] Della Corte G, Mazzolani FM. Theoretical developments and numerical verification of a displacementbased design procedure for steel braced structures. Proc. 14th world Conf. Earthq. Eng., Beijing: 2008.

[60] Pinho R, Casarotti C, Antoniou S. A comparison of single-run pushover analysis techniques for seismic assessment of bridges. Earthq Eng Struct Dyn 2007. https://doi.org/10.1002/eqe.684.

[61] Dwairi H, Kowalsky MJ. Implementation of inelastic displacement patterns in direct displacement-based design of

continuous bridge structures. Earthq Spectra 2006;22:631–62. https://doi.org/10.1193/1.2220577.

[62] Celik OC, Ellingwood BR. Seismic fragilities for non-ductile reinforced concrete frames - Role of aleatoric and epistemic uncertainties. Struct Saf 2010;32:1–12. https://doi.org/10.1016/j.strusafe.2009.04.003.